Available online at www.sciencedirect.com
SCIENCE DIRECT®
International Journal of Thermal Sciences 44 (2005) 694–708
International Journal of Thermal Sciences
www.elsevier.com/locate/ijts

# Heat transfer in a twin-blow narrow channel with two opposite walls roughened by skewed ribs arranged in staggered manner

S.W. Chang [a,*], K.F. Chiang [b], T.L. Yang [c], P.H. Chen [d]

[a] *Thermal Fluids Laboratory, National Kaohsiung Marine University, No. 142, Hai-Chuan Road, Nan-Tzu District, Postcode: 811, Kaohsiung, Taiwan, Province of China*
[b] *Graduate School, Department of Mechanical Engineering, National Taiwan University, Taiwan, Province of China*
[c] *Department of Electrical Engineering, Fortune Institute of Technology, Taiwan, Province of China*
[d] *Thermal MEMS Laboratory, Department of Mechanical Engineering, National Taiwan University, Taiwan, Province of China*

Received 14 January 2004; received in revised form 21 May 2004; accepted 21 May 2004

Available online 25 March 2005

**Abstract**

This experimental study performs the detailed heat transfer measurements over a skewed-rib roughened surface in a rectangular narrow channel with two equal-area flow entrances located on two adjacent edges of a channel-corner. This flow configuration allows for increasing the coolant-flow fed into the narrow channel without increasing the height of assembly in order to enhance the capacity of cooling duty for electronic chipsets. At a specified total coolant mass flow rate, four test scenarios, namely the single-blow from the side or upper entrance and the twin-blow with the coolant mass flow ratio of 1 : 1 or 2 : 1 between the side and upper blows are performed. A selection of full-field heat transfer distributions over the rib-roughened surface illustrates the manner by which the flow entry condition and the Reynolds number affect the local and spatially averaged heat transfers. With fixed total coolant consumptions, the twin-blow with the coolant mass flow ratio of 2 : 1 between the side and upper blows elevates the spatially averaged heat transfers to the levels of 150–180% of the single-blow references. A regression-type analysis is subsequently performed to develop the correlation of spatially-averaged Nusselt numbers over rib-roughened surface, which permits the effect of Reynolds number on heat transfer to be determined for four test scenarios.


*Keywords:* Twin-blow; Ribbed; Narrow; Channel

## 1. Introduction

Heat transfer in a rib-roughened channel has been a long term research subject for a variety of industrial applications such as turbine blade cooling, enhanced fin assembly and heat exchanger. Theses rib-roughened channels take varying cross-sectional shapes with a wide range of rib geometries typical of rib-angle 30°–90°, rib-height 0.0625–0.15 of channel-hydraulic-diameter and rib-pitch 8–30 of rib-height that are formulated as continuous, broken and V shaped with inline, staggered and criss-cross arrangements [1–11]. The studies of heat transfer in a rib-roughened narrow channel with the channel width-to-height ratios in the range of 6–10 are relatively rare although this flow configuration features the typical cooling passage in a plate-type heat exchanger [11]. As the past research efforts focused on the channels with width-to-height ratios of about 2–0.25, the rib-effects were mostly identified on near wall flow structures. These identified mechanisms associated with surface ribs which attribute to heat transfer augmentation involve the periodically broken boundary layers, the promotions of near-wall turbulence intensity and near-wall mixing and/or the rib-induced cross-stream secondary flows [1–11]. The implementation of rib-roughened channels for cooling of electronic chipsets with intensified circuit densities in a *Notebook PC* is strictly confined by the available machine height. A thin-wide ribbed channel becomes a remained option that

* Corresponding author. Tel.: +886 7 6126256; fax: +886 7 5712219.
*E-mail address:* swchang@mail.nkimt.edu.tw (S.W. Chang).

1290-0729/$ – see front matter 
doi:10.1016/j.ijthermalsci.2004.05.005

**Nomenclature**

| | | | |
|---|---|---|---|
| $A, n$ | correlative coefficients | $Re_s$ | Reynolds number based on side-blow mass flow rate |
| $B$ | channel gap ..... m | $Re_u$ | Reynolds number based on upper-blow mass flow rate |
| $d$ | hydraulic diameter of test channel ..... m | $T_w$ | local wall temperature at rib-roughened heating surface ..... K |
| $e$ | rib height ..... m | $T_f$ | reference fluid temperature ..... K |
| $H$ | length of test channel ..... m | $W$ | width of test channel ..... m |
| $k_f$ | thermal conductivity of coolant .. $W{\cdot}m^{-1}{\cdot}K^{-1}$ | $x, y$ | coordinates in streamwise and spanwise directions ..... m |
| $l$ | rib land ..... m | $X, Y$ | dimensionless streamwise and spanwise coordinates $(x/d, y/d)$ |
| $\dot{m}$ | total coolant mass flow rate ..... $kg{\cdot}s^{-1}$ | | |
| $Nu$ | local Nusselt number over rib-roughened fin surface, $= \frac{qd}{k_f(T_w-T_f)}$ | *Greek symbols* | |
| $Nu_a$ | spatially averaged Nusselt number over rib-roughened surface | $\alpha$ | attack angle of skewed rib ..... degree |
| $P$ | rib pitch ..... m | $\mu$ | dynamic viscosity of coolant ..... $kg{\cdot}s^{-1}{\cdot}m^{-1}$ |
| $q$ | convective heat flux ..... $W{\cdot}m^{-2}$ | | |
| $Re$ | Reynolds number based on total mass flow rate, $= \frac{\dot{m}d}{\mu(B\times W)}$ | | |

results in the large channel width-to-height ratio. When the two opposite rib-roughened walls are very close, the considerable and asymmetrical shear strains, induced by the staggered surface ribs, attribute to vorticity generation that could lead to large-scale and dynamic vortical flow structures. These time-varied vortical flow motions significantly affect the main flow structures in the narrow channel, creating a vortex-drafting like behavior and enhanced local vorticity for further heat transfer augmentation [12]. Also affected by the limited height available in a notebook PC is the prohibition of increased pumping-power for cooling by employing a large fan-assembly. To cope with these engineering specifications and the ever mounting cooling duty required for an electronic chipset, especially a CPU, the design concept of a rib-roughened narrow channel with twin-blow entrances that enables the increase of coolant flow by fitting two thinner fans at two entrances is formulated as shown in Fig. 1. The coolant is pressurized in two separated fans and fed into the rib-roughened narrow channel from the upper and side entrances. In addition to the required large channel width-to-height ratios in the range of 6–10 for present application, the flow structures and heat transfer characteristics in a twin-blow narrow channel are considerably modified from the conventional single-blow scenarios. Although the heat transfer enhancement using surface ribs has been a subject of much fundamental research over the last two decades [1–11], no previously published work is available for the rib-roughened channel with twin blow entrances. In this respect, the absence of research efforts and the need for electronic cooling in a notebook PC have motivated the present study.

## 2. Experimental details

### 2.1. Apparatus

The experimental apparatus is shown in Fig. 2. The test fluid, pressurized air, was directed into a rib-roughened narrow channel (1) from its upper and/or side entrances through two 350 mm long, smooth-walled, flow-calming sections (2)

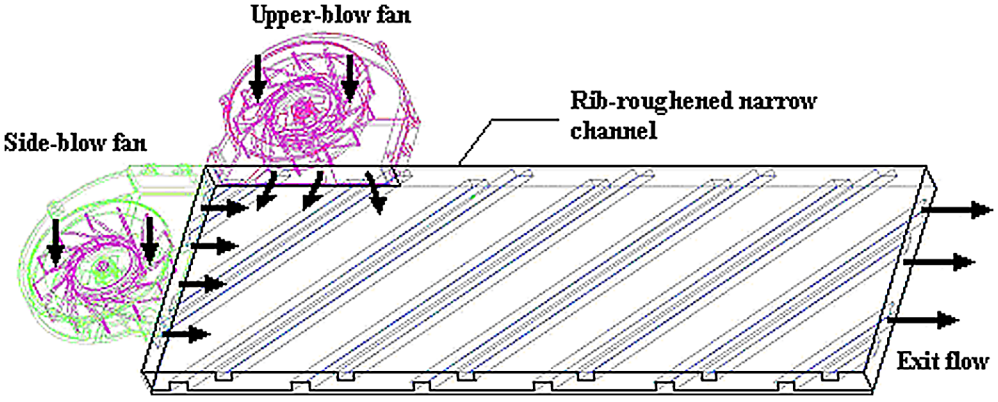


Fig. 1. Cooling assembly of twin-blow rib-roughened narrow channel.

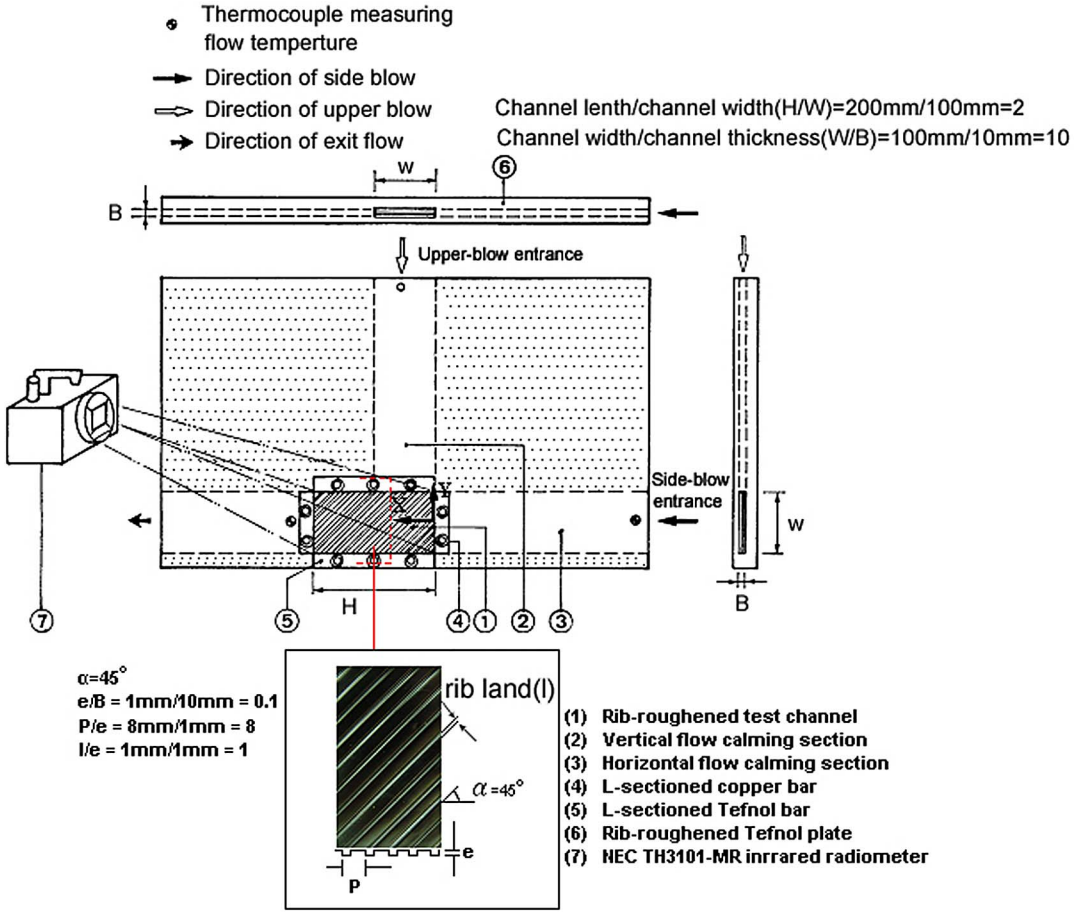


Fig. 2. Experimental apparatus.

and (3) of identical crossed section with test channel (1). Dimensions of test channel were 100 mm × 200 mm × 10 mm which gives a channel aspect ratio of 10 and the hydraulic diameter of 18.18 mm. Two flow calming sections were constructed by Teflon plates that respectively connected to the upper and side entry-edges of the test section. A $K$-type thermocouple penetrated into each of these two calming sections adjacent to the entrance of test channel that measures the coolant entry temperature. The flow entry temperature was treated as the fluid reference temperature to define the fluid properties at the flow entrance, such as the specific heat, thermal conductivity and viscosity of coolant, for the evaluation of Reynolds and Prandtl numbers at each flow entrance. At the exit-end of rib-roughened channel, three type $K$ thermocouples, positioned with equal spanwise interval, penetrated into the core of exit guiding section to measure the flow exit temperature. The flow exit temperature was used to check for the accuracy of energy accountancy based on the enthalpy balance method. Also the flow temperature at the exit plane of test section was calculated based on the net convective heat flux and total coolant mass flow rate, which value was constantly checked with the experimental measurement to assure the difference was limited less than 10%.

The repeated full skewed ribs were arranged in a staggered manner on two wide opposite walls of test channel. One of these two rib-roughened surfaces was electrically heated and produced by forging a continuous 0.1 mm thick stainless-steel foil into the geometry specified in terms of five non-dimensional groups defined in Fig. 2 of:

- Rib attack angle $(\alpha) = 45°$;
- Rib height/channel gap ratio $(e/B) = 1$ mm/10 mm $= 0.1$;
- Rib pitch/rib height ratio $(P/e) = 8$ mm/1 mm $= 8$;
- Rib land/rib height ratio $(l/e) = 1$ mm/1 mm $= 1$.

As there is heat conduction in the heated wall, it is inevitable to encounter wall-conduction effect which affects the spatial distributions of heat flux and wall temperature. Instead of the uniform heat flux generated by the electricity fed through the stainless steel foil, certain degree of non-uniformity in heat flux distribution could be attributed by the wall conduction effect. Also the wall conduction could smooth out the wall temperature distributions among the rib-bing region. The heat transfer coefficients were consequently smoothed by wall-conduction. Therefore, it is attempted to minimize the wall conduction effect by using the 0.1 mm heating foil. In addition, the perfect uniform heat flux condition is not feasible to be generated due to the external heat loss, which will be further addressed in the section dealing

with the program and data reduction. As indicated in Fig. 2, the origin of coordinate system, which involves the streamwise ($X$) and spanwise ($Y$) coordinates, was allocated at the middle span of side entry edge. Two $L$-sectioned copper bars (4) that connected the electrical terminals with the heating foil were secured on two side edges of the stainless-steel foil to form a complete electrical circuit. The adjustable high-current DC electrical power was fed directly into the heating foil to generate the basically uniform heat-flux heating surface. Along the other pair of horizontal edges of test section, two Tefnol-made $L$-sectioned bars (5) were fitted to secure the heating foil and prevent leakage. The identical rib-feature as the stainless-steel heating foil was machined on the Teflon plate (6) opposite to the heating foil and arranged in the staggered manner. Prior to entering each flow calming section, the air fed from the IWATA SC 175C screw-type compressor unit was dehumidified and cooled to the ambient temperature through a refrigerating unit. The dry and cooled airflow directed toward each of the two flow entrances was channeled through a set of pressure regulator and filter with the mass flow rate to be metered and adjusted by the Tokyo Keiso TF-1120 mass flow meter and the needle valve respectively. A digital-display pressure transducer measured the pressure level of coolant flow in each flow calming section. The wall temperatures over the heating surface were imaged by a calibrated two-dimensional NEC TH3101-MR infrared radiometer (7). This thermal image processing system could complete a full-field of $239 \times 255$ matrix scan in 0.3 seconds. The back surface of heating foil was painted black in order to minimize the background reflection and to increase the emission.

### 2.2. Program and data processing

Heat transfer tests over the rib-roughened surface with the single-blow from side entrance were initially performed as the baseline study. The test results acquired from the second phase using single-blow from upper entrance against which the baseline results were compared to unravel the impacts of flow entry condition on heat transfer. The third phase of program examined the heat transfer scenarios of twin blows with the coolant mass flow ratios of 1 : 1 and 2 : 1 between the side and upper blows. With the coolant to be fed from the side and/or upper entrances, the rate of coolant mass flow into each entrance was used to define $Re_s$ and $Re_u$, which respectively quoted for the Reynolds numbers of side and upper entrances. A number of Reynolds numbers from 500–6000 based on the total coolant mass flow rates in the range of 0.000506–0.00564 $\mathrm{kg{\cdot}s^{-1}}$ was tested for each blow condition. This selected Reynolds-number range covered the laminar and turbulent flows. The detailed heat transfer distributions over the rib-roughened surface at various Reynolds numbers with conditions of single and twin blows were examined. The manner by which the flow entry condition and Reynolds number affected the local and spatially averaged heat transfers was analyzed. Heat transfer correlations, which involved the controlling variable of Reynolds number evaluated from the total coolant mass flow rate, were subsequently derived for four flow entry conditions that permitted the determination of spatially averaged Nusselt numbers over rib-roughened surface for design application.

Steady state heat transfer measurements were performed at each set of predefined Reynolds number. The steady state was assumed when the variations of wall temperatures with several successive scans at the central spot of heating surface were less than 0.3 °C. Depending on the heating level and flow condition, the elapsed time to achieve the steady state was in the range of 30–45 minutes. Having satisfied the steady state assumption, the on-line infrared thermal-image data capture system was activated to record and transfer the full field wall temperatures over the heating surface into the PC. Along with the measured heating power and coolant entry temperature, $T_f$, the local Nusselt number distributions over the heating surface at the prescribed Reynolds number and entry condition were subsequently evaluated. The differences of $T_f$ values between the upper and side entrances for all the twin-blow test conditions examined were found less than 0.8% of $T_f$ value tested. Note, in order to compare the relative heat transfer performances between the results acquired from four different blow entry scenarios, the evaluation of Reynolds number was based on the total coolant mass flow rate and the hydraulic diameter of test channel. The various heat fluxes fed into the heating foil could also affect the Reynolds number even if the total amount of coolant mass flow rate remained invariant due to the thermal impact on fluids properties. Therefore, by adequately adjusting the coolant mass flow rate to compensate the varied fluid properties, the maximum variation in Reynolds number at the entry plane(s) of test channel was controlled with ±1% for each targeting value.

The local Nusselt number, $Nu$, are evaluated using the equation of

$$Nu = \frac{qd}{k_f(T_w - T_f)} \tag{1}$$

in which the convective heat flux, $q$, was obtained by subtracting the external heat loss from the electrical dissipation measured over the heating surface. It is worth noting that the heating surface adopted for heat-flux evaluation included two side profiles of each skewed rib. The characteristics of external heat loss at different heating levels were determined by a number of heat loss calibration runs. Each set of calibration test runs was performed with the flow blocked off. The fiberglass thermal insulating material was filled in the flow passage. The heat supplied to the heating foil was entirely lost so that the supplied heating power was balanced with the external heat loss at the corresponding steady-state temperature distribution. Due to the uniformities of the heat flux over heating surface and the thermal insulation inside test channel, the wall temperatures over the scanning area were found to distribute uniformly over the heating surface for each heat loss calibration run. A review

of the temperature data collected from the entire calibration test runs showed the less than 2.98% of non-uniformity in the wall temperature distributions. The plot of heat-loss flux against the corresponding steady wall-to-ambient temperature difference revealed a linear-like functional relationship, which correlated the heat loss flux with the local wall-to-ambient temperature difference. As the flow field inside the rib-roughened channel generates spatial heat transfer variations, the local wall temperatures varied spatially. Therefore the external heat loss remained as a spatial function that resulted in the non-uniformity of heat loss distribution and has yielded the perfect uniformity of convective heat flux over the rib-roughened surface. Having determined the local convective heat flux, the local Nusselt number, *Nu*, was subsequently defined using Eq. (1) with the thermal conductivity of coolant evaluated from the reference fluid temperature, $T_f$. For each heat transfer test run, heater powers were adjusted to raise the central-spot wall temperatures to the levels of 323, 333, 343, 353 and 363 K. This attempt was aimed at varying the buoyancy level and identified the degree of buoyancy impact on heat transfer. Within the present parametric ranges tested, the variations of buoyancy level could only produce the maximum heat transfer variations of about $\pm 3.8\%$ so that the buoyancy interaction on heat transfer was treated as negligible for present study. Also worth noting that the measured temperature contours from the back side of stainless steel foil were slightly higher than those at the fluid-wall interface. The one-dimensional Fourier conduction law was applied to correct the wall temperature measurements from the back-side of foil into the fluid-wall interface with the local heat flux evaluated as local convective heat flux, $q$.

The experimental repeatability of temperature measurement using NEC TH3101-MR infrared radiometer was carried out prior to the baseline experiments. The maximum variations of wall temperature measurements compared to the thermocouple measurements acquired from Fluke Net-Daq data logger with the test conditions to repeatedly reach the same steady states were in the range of $\pm 0.7\,^{\circ}\mathrm{C}$. By treating the maximum uncertainty of temperature measurement as $\pm 0.7\,^{\circ}\mathrm{C}$, which was the major source to attribute the uncertainties of coolant's thermal conductivity, fluid density and viscosity, the maximum uncertainty associated with the local Nusselt and Reynolds numbers were estimated to be 16.7 and 6.6%, respectively using the policy of ASME on reporting the uncertainties in experimental measurements and results [13].

## 3. Results and discussion

### 3.1. General observations

The heat transfer characteristics of rib-roughened test channel with four entry conditions are illustrated and compared using the results obtained at Reynolds number of 4000. Fig. 3 shows the distributions of Nusselt number contours over rib-roughened surface and the corresponding *Nu* profiles along $X$ and $Y$ axes for four entry conditions of single side-blow, single upper-blow and twin-blows of $Re_s = Re_u$ and $Re_s = 2Re_u$. Heat transfer results obtained with single side-blow shown in Figs. 3-a, 3-b and 3-c mostly reconfirm the typical skewed-rib effects on channel-flow heat transfer [2,3]. These repeated skewed ribs augment heat transfers to the levels about 2–3 times of Dittus–Boelter value [14]. As shown in Fig. 3-a, the spatial heat transfer distributions involve the streamwise "saw-tooth" pattern and the spanwise variation with the higher heat transfer rates developed along the upper portion of test channel as a result of the angled-rib induced swirling flow in the skewed direction of surface ribs. In Fig. 3-b where three streamwise heat transfer variations at spanwise locations of 1.25, 0 (centerline) and $-1.25$ are compared, three distinct heat transfer regimes, namely the entry, repeated-flow and exit regimes, respectively cover the regions of about $3 > X > 0$, $7 > X < 3$ and $10 > X > 7$. In the entry regime, the boundary-layer type developing flow is observed that shows the gradual streamwise heat transfer decay from the immediate entry level toward the "repeated flow" value. In this entry regime, the streamwise saw-tooth heat transfer variations remain vague and the Nusselt number curves along $Y = 1.25$, 0, and $-1.25$ axes tend to converge. The rib-associated flows along with boundary layers in the entry regime are under development. In the repeated-flow regime, heat transfers systematically decay from the upper-edge to the bottom-edge levels along each skewed rib. Accompanying with such rib-wise heat transfer variation is the repeatedly streamwise saw-tooth variations with the local peak developed at the top surface of each rib. In the exit regime, although the streamwise saw-tooth pattern is still appreciable, the systematic rib-wise heat transfer variations are disturbed due to the exit effect. The spanwise heat transfer variations in the entry, repeated-flow and exit regimes are respectively typified in Fig. 3-c by showing the Nusselt number variations along $Y$ axis at three streamwise spots of 1, 5, and 9 $X$. The systematically spanwise heat transfer decays from the highest levels along the upper-edge of heating foil ($Y = 2.5$) toward its bottom edge ($Y = -2.5$) are consistently found at the streamwise spots of 1 and 5 $X$. Along the span of $X = 9$ that falls in the exit regime, a spanwise heat transfer decay also initiates from the upper edge onto the centerline across which the moderate spanwise heat transfer recovery develops toward the bottom edge. It is worth noting that most of the skewed ribs in the entry and exit regimes are not in the complete lengths so that the heat transfer characteristics developed in the repeated-flow regime gradually vanish when the flow travels further downstream in the exit regime. Due to the incomplete skewed ribs that streamwisely weaken the rib-effects in the exit regime; the strength of swirling flows developed in the repeated-flow regime is weakened. The skewed-ribs induced vortex structures in the exit regime undergo a streamwise modification in the manner of generating the recirculation-type corner flows at the upper-left region as indicated by the close looped Nus-

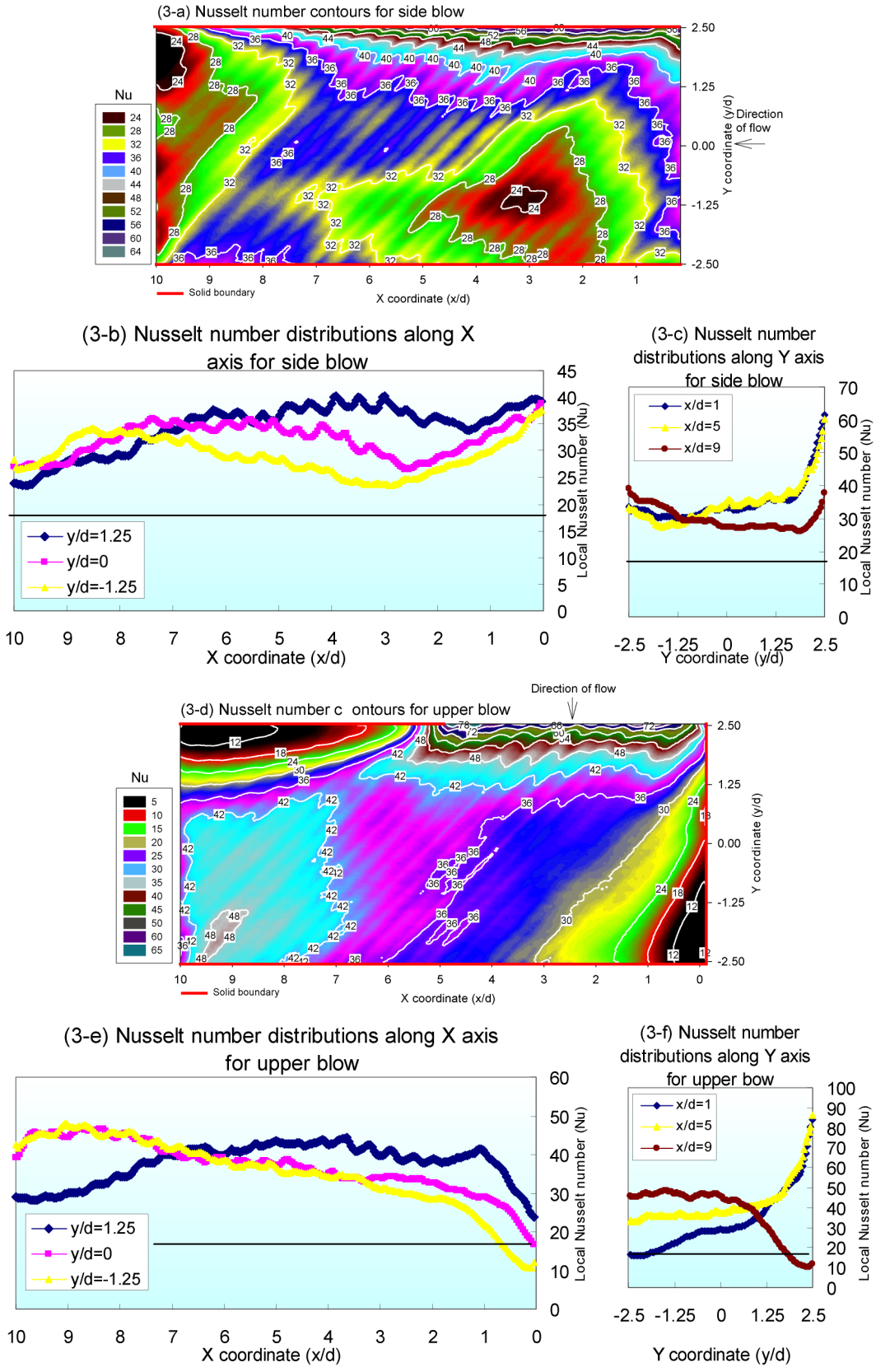


Fig. 3. Distributions of Nusselt number contour over rib-roughened narrow channel at Reynolds number of 4000. (—— Dittus–Boelter correlation level.)

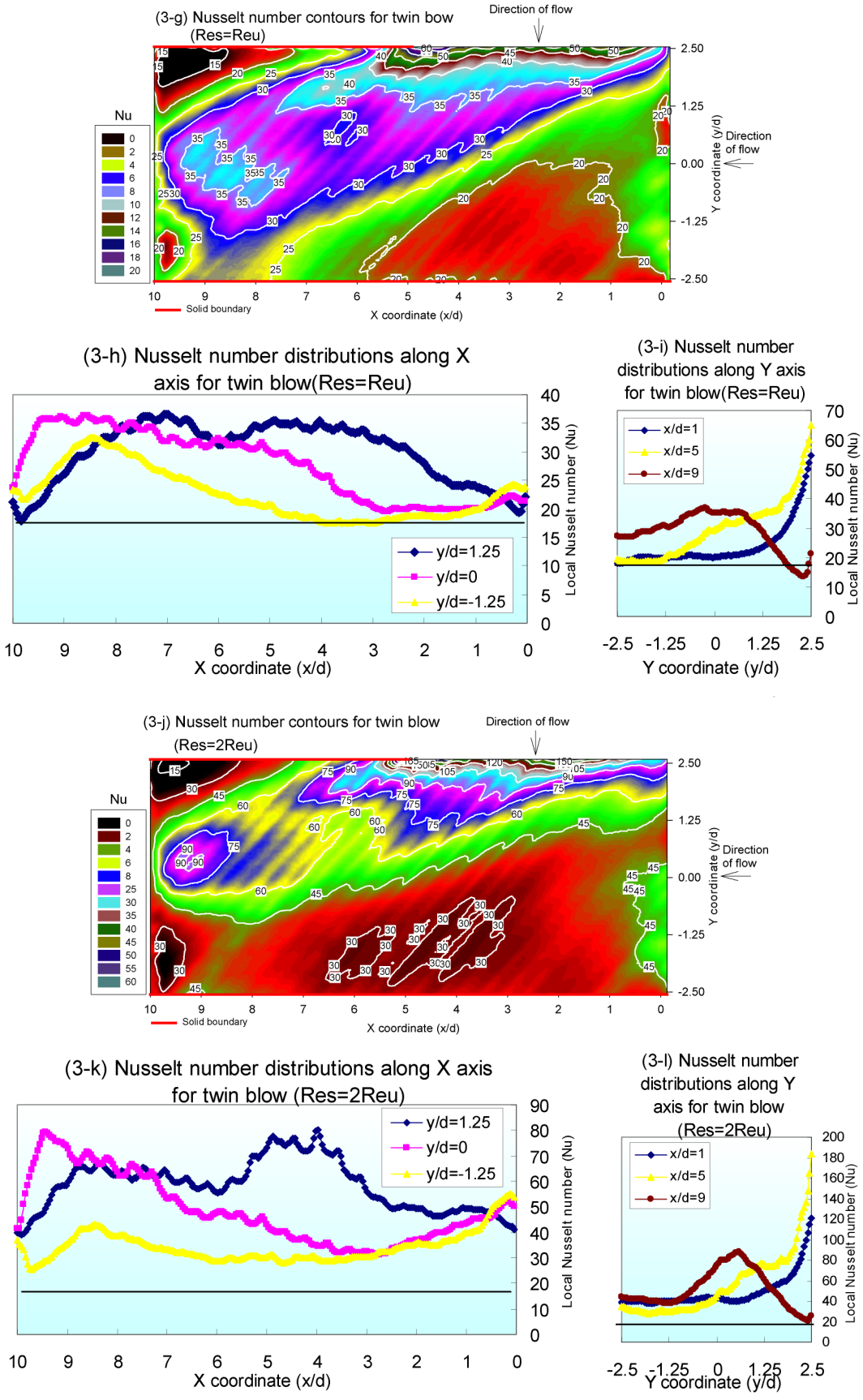


Fig. 3. (Continued).

selt number contours shown in Fig. 3-a. Nevertheless, for all the three curves collected in Fig. 3-c, the most significant heat transfer decays in the spanwise direction are consistently found in the region of about $1.8 < Y < 2.5$.

Figs. 3-d, 3-e and 3-f unravel the typical heat transfer results found for the single upper-blow entry condition. As shown in Fig. 3-d, the upper blow entry-effect produces a high heat transfer region adjacent to the upper-right entry-edge. A major and a minor flow re-circulation zones are identified via two closed-looped concave heat transfer surfaces that respectively develop on the upper-left corner and adjacent to the sealed right-side edge. These two close-looped vortices are induced by the turning movement of main bulk stream from the upper-right entrance toward the left-side exit. The typical rib-induced swirling flow found in the single side-blow scenarios, which washes the heated wall in the direction along the skewed ribs, is considerably modified by feeding the coolant stream from the upper-right entrance aimed at the left-end exit. It is noted in Fig. 3-d that the concave heat transfer surfaces over these two recirculation zones are rather "flat" relative to the "saw-toothed" regime found in the central core. The conventionally spatial heat transfer variations reported previously in the single side-blow channel [1–11] are replaced by the vortex-type characteristics in the recirculation regions (see Fig. 3-d). As a result, three distinct heat transfer regimes could be identified in Fig. 3-e as the minor vortex regime ($0 < X < 2.5$), rib-effective regime ($2.5 < X < 5.5$) and major vortex regime ($5.5 < X < 10$). A comparison of the results depicted in Figs. 3-b and 3-e shows that most of the streamwise heat transfer levels along $Y = -1.25$ axis are elevated from the single side-blow references, which phenomenon almost prevails over the entire lower portion of test channel. This regard is treated as a beneficial remark of using upper-blow in view of the heat transfer augmentation in angled-ribbed channel. The saw-tooth streamwise heat transfer variations are only observed in Fig. 3-e where $2.5 < X < 5.5$. The local heat transfers drop considerably when the fluids trap in the major and minor vortices, which could impede heat transfers to the levels close to the Dittus–Boelter value as compared in Figs. 3-e and 3-f. In this regard, the single side-blow condition could avoid the development of large-scale recirculation zones and the additional pumping power required to drive the turning motion of main bulk stream. The considerable amount of heat transfer improvement in the flow entry region is also demonstrated in Fig. 3-f in the spanwise region of about $1.8 < Y < 2.5$ along the axes of $X = 1$ and 5.

Justified by the heat transfer results collected in Figs. 3-d–f, the drawback and merit of single upper-blow entry condition are respectively the generation of re-circulating vortices and the relative heat transfer improvements from baseline study over the lower portion of test channel. Despite the fact that twin blows could offer the increased coolant mass flow by providing two flow entrances without the increase of total height of cooling assembly, the strategy of breaking the upper-entry induced vortex structures by introducing a side-blow stream is implemented with the aim for further heat transfer augmentation. Figs. 3-g–i and 3-j–l depict the heat transfer results obtained with twin blows at conditions of $Re_s = Re_u$ and $Re_s = 2Re_u$. A comparison of the corresponding plots for test results shown in Figs. 3-g–i and 3-j–l obtained at conditions of $Re_s = Re_u$ and $Re_s = 2Re_u$ reveals a considerable amount of similarities in the qualitative sense. The manners of heat transfer distribution over the rib-roughened surface for both twin-blow conditions are similar. But the heat transfer levels in the case of $Re_s = Re_u$ are considerably lower than the counterparts found with $Re_s = 2Re_u$. When the vertical and horizontal flow momentums are equal in magnitude for the case of $Re_s = Re_u$, the momentum components normal to the rib direction from the side and upper blows cancel out so that the heat transfer levels in the case of $Re_s = Re_u$ are reduced from the scenario of $Re_s = 2Re_u$. However, as shown in Figs. 3-g ($Re_s = Re_u$) and 3-j ($Re_s = 2Re_u$), the upper-blow entry regime found in Fig. 3-d is considerably skewed and extended due to the addition of flow momentums from the side and upper blows. This skewed high heat transfer entry region, initiated from the upper-right entry edge, occupies most of the upper portions over the rib-roughened surface. The momentums in side and upper blows, accompanied with the extended and skewed upper-entry region, provide synergistic impact on the "major" vortex-structure developed at the upper-left corner in the single upper-blow channel. The distributions of heat transfer contour over the channel's upper-left corner shown in Figs. 3-g and 3-j involve the small closed-looped region with appreciable rib-wise heat transfer reduction from upper to bottom channel-edges where the streamwise saw-tooth variations are present. The major vortex structure formulated in the single upper-blow channel is considerably shrunk and broken-down by introducing the side-blow for both twin-blow conditions. The streamwise heat transfer variations along 1.25, 0 and $-1.25$ $Y$ axes in these two twin-blow channels with conditions of $Re_s = Re_u$ and $Re_s = 2Re_u$ are respectively shown in Figs. 3-h and 3-k. The clear saw-tooth variation pattern, despite in the entry regime of side-blow entrance that is specified in the range about $0 \leqslant X \leqslant 2.5$, emerges for both twin-blow conditions. Unlike the results found in the single side-blow channel shown in Fig. 3-b, heat transfers along the streamwise axis of $Y = 1.25$ diverge from the two converged curves along $Y = 0$ and $-1.25$ axes in the side-blow entry regime among where the saw-tooth patterns are not appreciable due to the developing nature of rib-associated flows. The complex flow interactions between the side and upper blows, intervened by the skewed ribs, take place at the upper-right corner, which considerably enhance the entry-regime heat transfers. Heat transfers over the upper portion of channel, as typified by the data indicated along $Y = 1.25$ axis, are considerably amplified with the peak values developed among the central streamwise span for the case of $Re_s = 2Re_u$ (see Fig. 3-k). The weak heat transfer region in the lower-right corner of

single side-blow channel as shown in Fig. 3-d diminishes as a result of side-blow; that is replaced by a flow entry regime with a bandwidth of about 2.5 hydraulic diameters (see Figs. 3-g and 3-j). In the region of $5 \leqslant X \leqslant 10$, the streamwise heat transfer distributions depicted in Figs. 3-g and 3-j completely yield the single upper-blow scenarios but recover to the profiles found in single side-blow channel as revealed in Fig. 3-a. The spanwise heat transfer variations along the $X = 1$ and 5 axes and along the $X = 9$ axis shown in Figs. 3-i and 3-l respectively recast the patterns obtained with the entry conditions of single side-blow and single upper-blow. A cross examination of the heat transfer data acquired along the axis of $X = 9$ between Figs. 3-j and 3-f demonstrates the considerable heat transfer elevation over the major vortex region in the twin-blow channel of $Re_s = 2Re_u$. Thus the vortex break-down triggered by the side-blow with non-equal flow momentums between upper and side blows, which could enhance the vorticity by introducing asymmetrical shear strains in the narrow channel, has demonstrated its enhancing impact on local heat transfers. The above described heat transfer characteristics identified from the channels with single side and upper blows and with two twin blows are typical for all the test results but the degrees of entry impacts on heat transfer vary with Reynolds number.

### 3.2. Reynolds number impacts

The heat transfer results typified in Fig. 3 unravel the impact of flow entry condition on local heat transfers in a rib-roughened narrow channel. Due to the various flow fields generated in the channel, the impact of total Reynolds number on overall heat transfers varies with flow entry condition. Figs. 4, 5, 6 and 7, respectively, collect the heat transfer results obtained at total Reynolds numbers of 500,

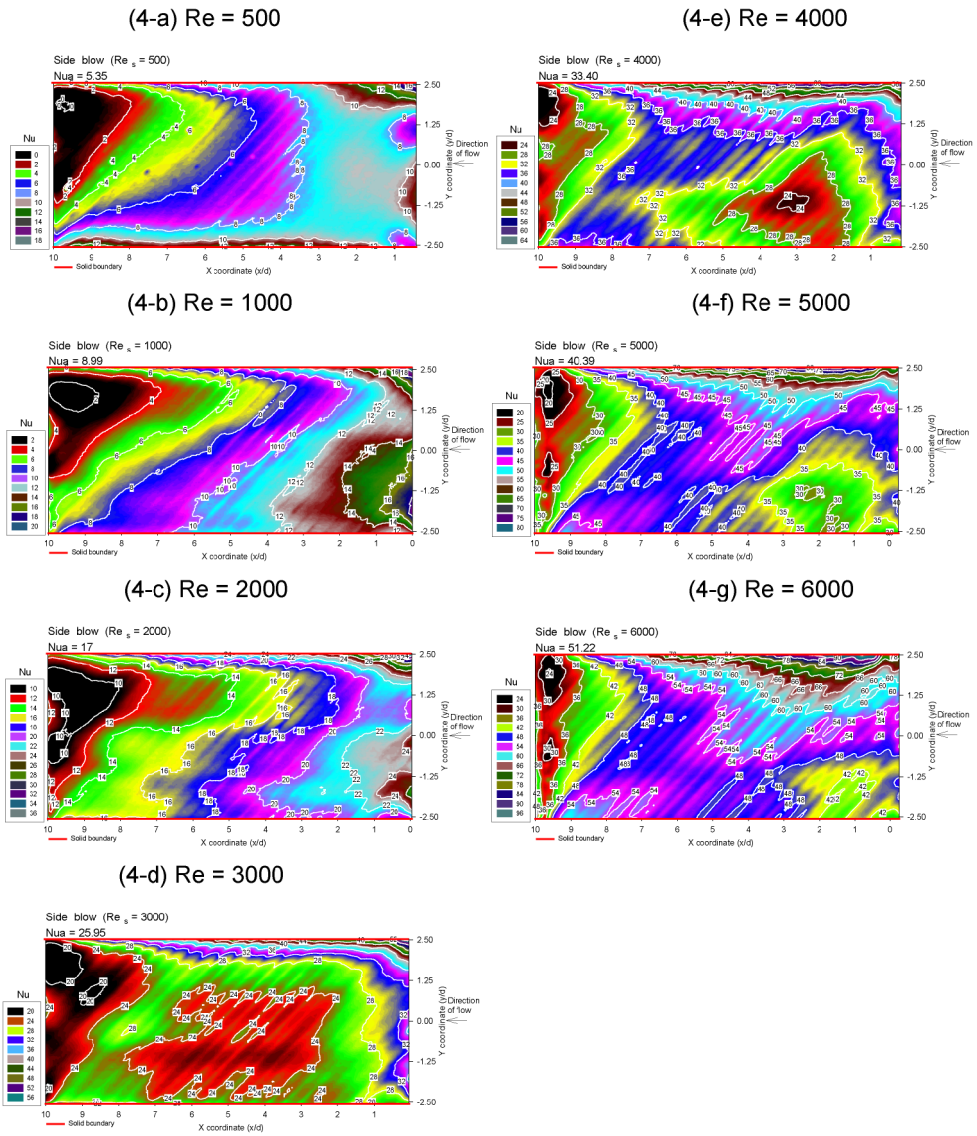


Fig. 4. Distributions of Nusselt number contour over rib-roughened narrow channel for side-blow entry at Reynolds numbers of 500, 1000, 2000, 3000, 4000, 5000 and 6000.

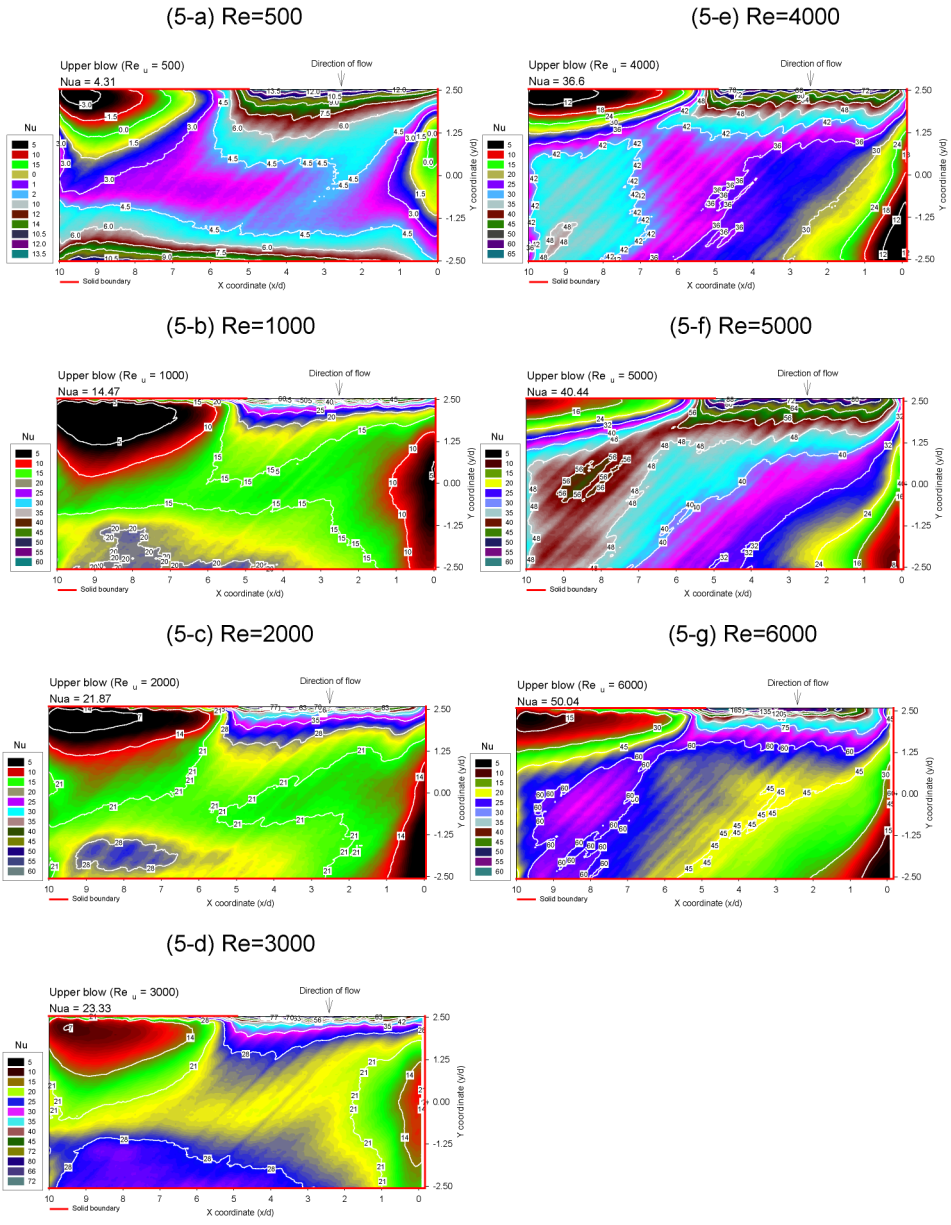


Fig. 5. Distributions of Nusselt number contour over rib-roughened narrow channel for upper-blow entry at Reynolds numbers of 500, 1000, 2000, 3000, 4000, 5000 and 6000.

1000, 2000, 3000, 4000, 5000 and 6000 with single-side and single-upper blows and for two twin-blow conditions of $Re_s = Re_u$ and $Re_s = 2Re_u$. As a reference scenario, the Nusselt number distributions over rib-roughened surface with single side-blow depicted in Fig. 4 mostly recast the typical heat transfer results found in a rectangular channel fitted with skewed surface ribs [9]. Rib-wise heat transfer decay from the upper edge toward the bottom edge of rectangular channel prevails over the rib-roughened surface, which is accompanied with the streamwise saw-tooth variation pattern with local heat transfer peak developing on each top-face of rib. The increase of Reynolds number from 500 to 6000 enhances the rib-associated effects on heat transfer by triggering the more clearly rib-wise and streamwise heat transfer variations. With Reynolds numbers less than 3000 as shown in Figs. 4-a, 4-b and 4-c, the streamwise saw-tooth patterns are not yet clearly emerged on the heat transfer surfaces but the rib-induced swirls have already provided appreciable impact on heat transfer by inducing the evident rib-wise heat transfer variations. Following the systematic increase of Reynolds number from 500 to 6000, the high-heat-transfer region gradually shifts from the side entrance at Reynolds number of 500 toward the upper-middle region when the Reynolds number reaches 6000. With conditions of $Re > 3000$, the spatial region where the Nusselt number levels exceed the entrance values has already developed at the upper-middle region of the rectangular channel. Referring to the previous statements illustrating Fig. 3-a,

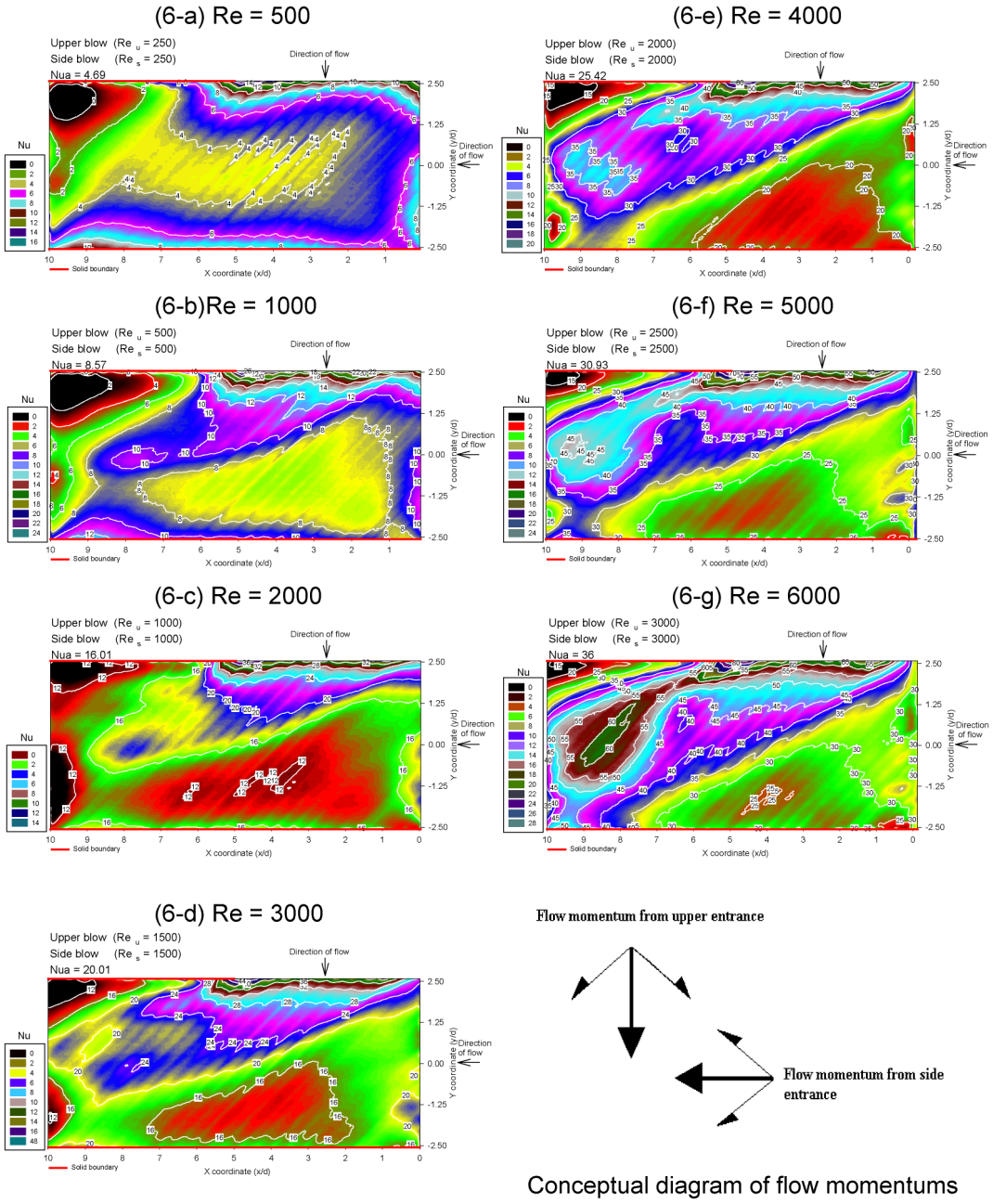


Fig. 6. Distributions of Nusselt number contour over rib-roughened narrow channel for twin-blow entry of $Re_s = Re_u$ at Reynolds numbers of 500, 1000, 2000, 3000, 4000, 5000 and 6000.

the area subject to the profound rib-impact is located at the middle region of the rectangular channel due to the incomplete rib lengths in the exit region and the developing nature of rib-flows adjacent to the flow entrance. Therefore the trend of spatial heat transfer variation depicted from Figs. 4-a to 4-g reflects the enhancing rib-impact on heat transfer due to the increased Reynolds number. The spatially averaged Nusselt numbers, $Nu_a$, correspondingly increase when the Reynolds number increases systematically.

When the coolant is fed from the upper entrance at Reynolds number of 500 as shown in Fig. 5-a, the 90° turning motion of main stream induces two concave heat transfer surfaces at the upper corner of flow exit and at the location adjacent to the sealed side edge. Along the bottom edge upon where the coolant stream impinges as unraveled in Fig. 5-a, a horizontal narrow band with high heat transfer rates develops so that the typical rib-wise heat transfer variations found in the single-side-blow channel vanish. A systematic increase of Reynolds number from 500 to 3000 incurs a corresponding shrinkage for the concave heat transfer surface along the sealed side-edge; while the bandwidth of high heat transfer region along the bottom channel-edge gradually extends toward the interior of rib-roughened channel. Further

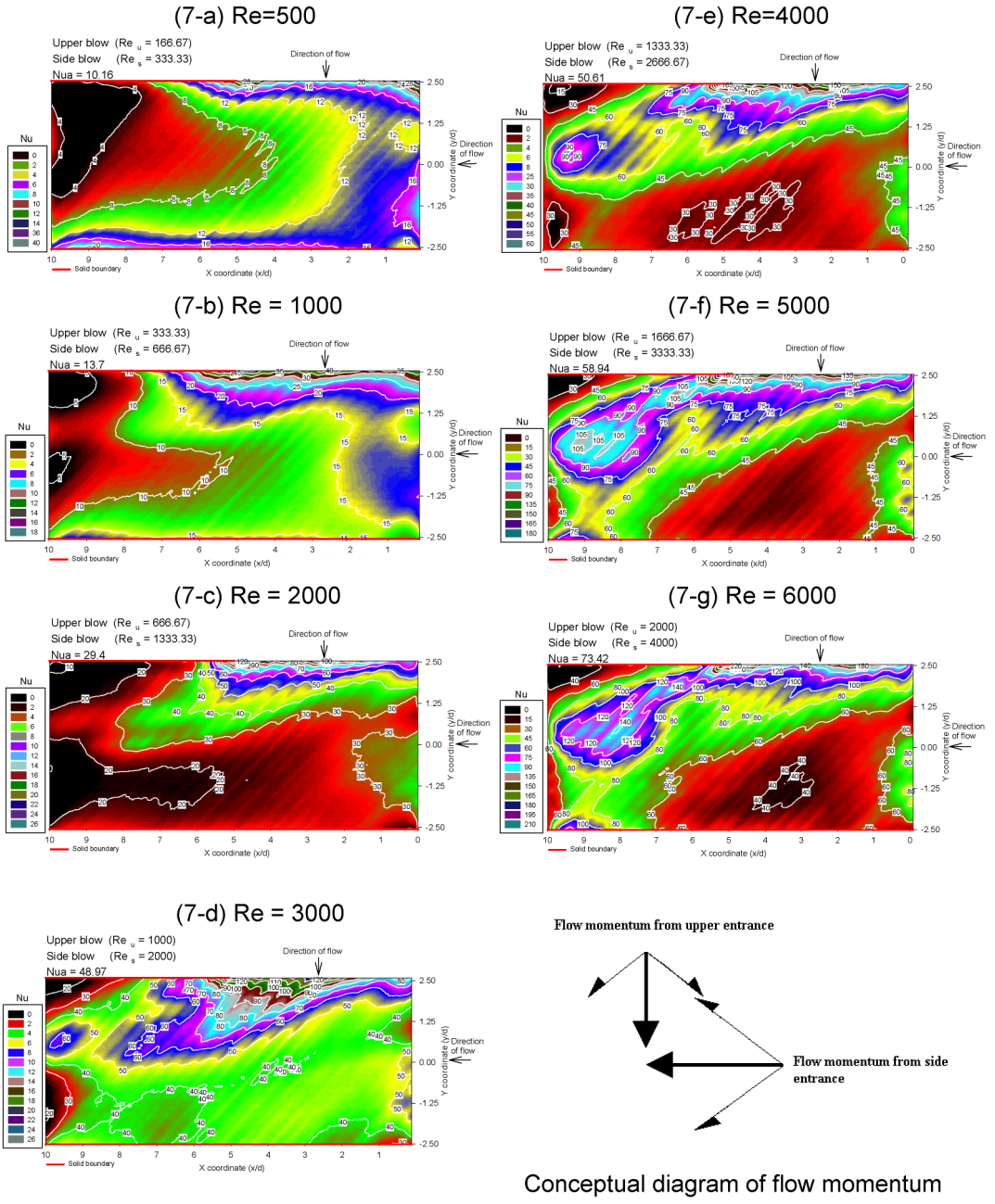


Fig. 7. Distributions of Nusselt number contour over rib-roughened narrow channel for twin-blow entry of $Re_s = 2Re_u$ at Reynolds numbers of 500, 1000, 2000, 3000, 4000, 5000 and 6000.

increase of Reynolds number from 3000 to 6000, the locally high heat transfer region along the bottom channel-edge disappears and the region of concave Nusselt number surface at the upper exit corner shrinks. Unlike the results unraveled in Figs. 4-e, 4-f and 4-g for side-blow channel, the heat transfer surfaces among the lower corner of sealed side-edge gradually smooth out without the appearance of streamwise zigzags when the Reynolds number increases from 4000 to 6000. A strong skewed stream-flow from the upper-right entrance is guided by these skewed surface ribs that directs toward the lower exit edge, creating a wide skewed high-heat-transfer band along the diagonal of rectangular channel. Within this wide skewed band, the zigzag streamwise heat transfer variations appear with locally high heat transfer rate on each rib location as shown in Figs. 5-e, 5-f and 5-g. The streamwise saw-tooth heat transfer variations are vaguely present in both upper-left and lower-right corner regions where the re-circulating flows prevail. The $X$-wise span of the recirculation area along the upper channel-edge, which initiates at the spot immediately adjacent to the upper entrance, is not affected by the increased Reynolds number. However, the spatially averaged Nusselt number, $Nu_a$, steadily increases with the increased Reynolds number.

For the twin-blow scenarios, the increase of total Reynolds number results in the simultaneous enhancement of flow momentums from the side and upper entrances. Fig. 6 depicts the systematic heat-transfer variations due to the increase of total Reynolds number from 500 to 6000 at the condition of $Re_s = Re_u$. For all the Reynolds numbers tested as seen in Fig. 6, the re-circulating flow regime persistently remains at the upper-left corner within which the rib-induced heat-transfer zigzags diminish. The side-blow for each twin-blow case shown in Fig. 6 eliminates the flow recirculation adjacent to the side-entrance found in the single upper-blow scenarios. At Reynolds number of 500, a "⊐" shaped high-heat-transfer opened-ring surrounds the upper and side entrances and the bottom channel-edge. Adjacent to the heat transfer regime confined by the "⊐" shaped opened-ring is a concave heat transfer surface at the upper-left exit corner that dominates by the 90°-turn induced re-circulating flow. Further increase of Reynolds number from 500 to 6000, a tendency of separating heat transfers into two distinct regimes over the rib-roughened channel gradually emerges, indicated by the appearance of a diagonal isotherm with constant *Nu* values. The locations above the diagonal heat transfer isoline involve the upper entrance region, the upper-left corner vortex and a skewed stream. Heat transfers within the bandwidth of the skewed stream positioned above the diagonal *Nu* isoline experience both the rib-wise variations and the streamwise zigzags. As the Reynolds number increases from 2000 to 6000, a close-looped high heat transfer region gradually evolves at the location between the upper-left-corner concave *Nu* surface and the diagonal *Nu* isoline. In this regard as labeled in Fig. 6-g at Reynolds number of 6000, the local Nusselt number peaks reach about 60 in the close-looped enhancing region above the diagonal *Nu* isoline. This close looped heat transfer peaks are likely a consequence of the development of counter-rotating vortices adjacent to the upper-left-corner vortex. The improved heat transfer in this close-looped region implicitly reflects the unstable vortices in contrast to the impeding results developed in the upper-left-corner vortex. Although the rich flow structures are triggered by a systematic increase of Reynolds number from 500 to 6000 as demonstrated in Fig. 6, the Nusselt number levels are generally less than the counterparts in Figs. 4 and 5. This is due to the equal magnitude of flow momentum between upper and side blows. As indicated by the conceptual diagram illustrating the addition of flow momentums from the upper and side entrance, the momentum components normal to the rib direction from the upper and side entrances cancel out each other that absent themselves from traversing the skewed ribs. Consequently, in comparison to the counterparts shown in Fig. 4 for single side-blow condition, the rib-effects found in the twin-blow channel for the regime below than the diagonal *Nu* isoline are moderated. Heat transfers in this flow regime below than the diagonal *Nu* isoline show no sign of vortical flow structure but the typical *Nu* surface with zigzag patterns.

Although the introduction of twin-blow concept could moderate the heat transfer impediment associated with re-circulating vortices and triggers a close-looped heat transfer augmenting regime, the cancellation of momentum components in the direction normal to the rib unravels heat transfer reduction from the single-blow scenarios. This has led to the development of a twin-blow system with non-equal magnitude between side and upper blows. Fig. 7 collects the heat transfer surfaces measured at Reynolds number of 500–6000 at the condition of $Re_s = 2Re_u$. As indicated in the conceptual diagram of flow momentums from the side and upper entrance, the net momentum component in the direction normal to the rib is oriented toward the upper-left corner. As a result, the *Nu* diagrams collected in Fig. 7 share similar distributing patterns with the counterparts of Fig. 6 but the diagonal *Nu* isoline developed in Fig. 6 and its associated flow structures are "squeezed" toward the upper-left corner. The close-looped heat transfer improving region positioned above the diagonal *Nu* isoline is observed at Reynolds number of 3000 in Fig. 7-d, which regime is not clearly shown until Reynolds number reaches 5000 as shown in Fig. 6. Because the across rib traversing in the twin-blow scenarios of $Re_s = 2Re_u$ prevails that incurs the typical rib-impacts on heat transfer augmentation, the spatially averaged Nusselt number, $Nu_a$, for each individual plot of Fig. 7 is considerably elevated from the condition of $Re_s = Re_u$, which level also exceeds each counterpart found in the single side and upper blows. The scenarios consistently provide the highest overall heat transfer levels within the present test conditions are found in the twin-blow channel with $Re_s = 2Re_u$.

### 3.3. Heat transfer correlation

For engineering applications, it is essential to evaluate the convective capabilities over the rib-roughened surface for a given total coolant consumption in order to determine the cooling duty available. Therefore the local Nusselt numbers over the rib-roughened surface generated with the entire total Reynolds numbers and entry conditions are spatially averaged to acquire the spatially averaged Nusselt number data $Nu_a$ for further data analysis aimed at disclosing its regressive-type equation. In the quest to identify the *Re* impact on the spatially averaged heat transfer $Nu_a$; four sets of data generated from test channels with single side-blow, single upper-blow, twin-blow of $Re_s = Re_u$ and twin-blow of $Re_s = 2Re_u$ are compared in Fig. 8 to illustrate the varying manner of $Nu_a$ against *Re*. It is clearly demonstrated in Fig. 8 that the spatially averaged Nusselt number, $Nu_a$, steadily increases with the increase of total Reynolds number for all the entry conditions examined. As compared in Fig. 8, the $Nu_a$ values for conditions of single-side and single-upper blows are in the similar levels. The twin-blow condition with $Re_s = Re_u$ reveals the lowest heat transfer levels among the four sets of test results due to the cancellation of momentum components normal to the rib direction which prevents themselves from traversing the skewed ribs. For the case

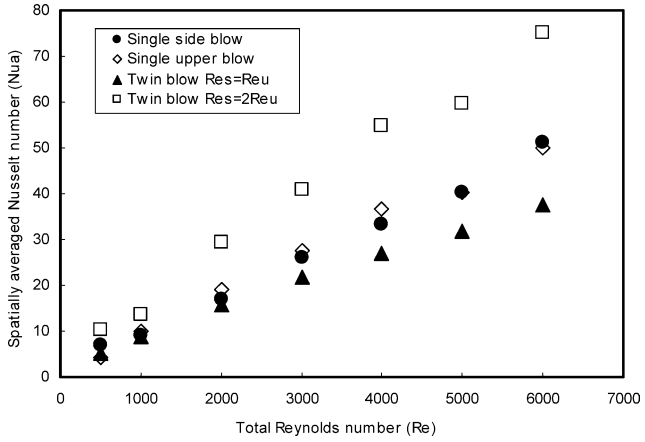


Fig. 8. Variation of spatially averaged Nusselt number with Reynolds number for side-blow, upper-blow and two twin-blow entry conditions.

Table 1
$A$ and $n$ coefficients for entry conditions of side, upper and twin blows

| Flow entry condition | $Nu_a = A \times Re^n$ | |
|---|---|---|
| | Coefficient $A$ | Coefficient $n$ |
| Single side-blow channel | 0.0811 | 0.7191 |
| Single upper-blow channel | 0.0169 | 0.9239 |
| Twin-blow channel with $Re_s = Re_u$ | 0.0338 | 0.8057 |
| Twin-blow channel with $Re_s = 2Re_u$ | 0.0531 | 0.8307 |

of $Re_s = 2Re_u$, the $Nu_a$ values for such twin-blow condition are in the range of 1.5–1.8 times of those counterparts obtained in the single-blow channel. The considerable heat transfer augmentation for rib-roughened narrow channel is confirmed by employing the twin-blow entry condition with $Re_s = 2Re_u$. Also proposed by the thermal physic of zero forced convective capability at the limiting case of $Re = 0$ is an asymptotic constraint of zero $Nu_a$ value when $Re$ approaches zero. Justified by all the versions of data trends revealed in Fig. 8 and considering the limiting case of $Re = 0$, the data trends shown in Fig. 8 for each entry condition are correlated by the equation of

$$Nu_a = A \times Re^n \text{ for each entry condition} \quad (2)$$

where the $A$ and $n$ functions are the numerically determined curve-fitting coefficients. In the range of $500 \leqslant Re \leqslant 6000$, the $A$ and $n$ coefficients in Eq. (2) are summarized in Table 1. A review for accuracy of Eq. (2) ensures that 96% of the entire experimental data agrees with the correlation results within $\pm 10\%$ discrepancies. Eq. (2) could be adopted as a design measure to evaluate the $Nu_a$ value over the narrow rib-roughened channel for four different flow entry conditions.

## 4. Conclusions

This experimental study is aimed at identifying an enhanced cooling measure for electronic chipset, which examines the heat transfer in a narrow rectangular channel with two opposite walls roughened by 45° ribs arranged in the staggered manner. Four sets of test results for single side-blow, single upper-blow and two twin-blows of $Re_s = Re_u$ and $Re_s = 2Re_u$ are illustrated to demonstrate the impact of flow entry condition and Reynolds number on heat transfer. In conclusion, the following observations emerge from the data generated by the present investigation.

(1) Heat transfer results with single side blow reconfirm the typical rib-effects on $Nu$ distributions which involve both "streamwise saw-tooth" and "rib-wise decay" variations over the rib-roughened surface. Three characteristic heat transfer regimes, namely the entry, repeated-flow and exit regimes, are distinguishable for each test scenario. Boundary-layer type developing flow is observed in the entry regime so that the streamwise zigzags and spanwise heat transfer variations are vaguely present. In the repeated flow regime, heat transfer variations follow the streamwise zigzag pattern and rib-wise decay. As the most of skewed-ribs are not complete in the exit regime, the rib-wise heat transfer variations are disturbed even if the streamwise saw-tooth pattern is still appreciable. Increase of Reynolds number amplifies the degree of rib-impacts on heat transfer with the characteristic heat-transfer feature remains unchanged.

(2) A major and a minor flow re-circulation zones, indicated by two smooth $Nu$ valleys, respectively develop on the upper exit corner and aside the sealed side entrance for single upper-blow condition. Local heat transfers in these two vortex-dominant regimes could be impeded to the levels about Dittus–Boelter values. The increase of Reynolds number from 500 to 6000 causes the high $Nu$ band along the bottom-edge of test channel to gradually extend toward the interior of channel and merge into the skewed central stream where the rib-effect is effective. Streamwise saw-tooth $Nu$ pattern only develops in this rib-effective regime among which the heat transfers over the lower portion are elevated from the single side-blow counterparts.

(3) A skewed high heat transfer regime, initiated from the upper-right entry edge and segregated above the diagonal $Nu$ isoline consistently develops in both twin-blow channels over which the streamwise zigzag and rib-wise decay prevail. The stream of side-blow traverses the turn-induced recirculation zone to trigger a vortex break-down process which consequences involve the extension of upper entry region and the generation of close-looped $Nu$ crests over the upper corner of channel exit. With conditions of $Re_s = Re_u$, the cancellation of momentum components in the direction normal to the rib weakens the traversing flow that has led to heat transfer reduction from the single-blow scenarios. Heat transfer results acquired from test conditions of $Re_s = 2Re_u$ that ensures the rib traversing flow are considerably improved from each of the single-blow chan-

nels. Rich flow structures are induced by the systematic increase of Reynolds number from 500 to 6000 for both twin-blow channels as unraveled in Figs. 6 and 7.

(4) The proposed $Nu_a$ correlation permits the effect of $Re$ on spatially averaged heat transfer over the skewed-ribs roughened surface to be evaluated for single side-blow, single upper-blow and two twin-blow conditions of $Re_s = Re_u$ and $Re_s = 2Re_u$. Among all the test results, the twin-blow case of $Re_s = Re_u$ features the worst heat transfer scenario while the $Nu_a$ values in the twin-blow channel of $Re_s = 2Re_u$ are in the range of 1.5–1.8 times of those counterparts obtained in the sing-blow channels which measure could be adopted for further heat transfer augmentation in rib-roughened narrow channel.

## References

[1] J.C. Han, J.S. Park, Measurement of heat transfer and pressure drop in rectangular channels with turbulence promoters, NASA contract report 4015, 1986.

[2] Y.J. Jang, H.C. Chen, J.C. Han, Flow and heat transfer in a rotating square channel with 45 deg angled ribs by Reynolds stress turbulence model, ASME J. Turbomachinery 123 (2001) 124–131.

[3] B.V. Johnson, J.H. Wanger, G.D. Steuber, F.C. Yeh, Heat transfer in rotating serpentine passages with trips skewed to the flow, ASME J. Turbomachinery 116 (1992) 113–123.

[4] T.M. Liou, J.J. Hwang, S.H. Chen, Simulation and measurement of enhanced turbulent heat transfer in a channel with periodic ribs on one principal wall, Internat. J. Heat Mass Transfer 36 (1993) 507–517.

[5] M.E. Taslim, T. Li, D.M. Kercher, Experimental heat transfer and friction in channels roughened with angled, V-shaped, and discrete ribs on two opposite walls, ASME J. Turbomachinery 118 (1996) 20–28.

[6] J.R. Shen, Z. Wang, P.T. Ireland, T.V. Jones, Heat transfer enhancement within a turbine blade cooling passage using ribs and combinations of ribs with film cooling holes, ASME J. Turbomachinery 118 (1996) 428–434.

[7] S. Mochizuki, A. Murata, M. Fukunga, Effect of rib arrangements on pressure drop and heat transfer in a rib-roughened channel with a sharp 180 deg turn, ASME J. Turbomachinery 119 (1997) 610–616.

[8] G. Rau, M. Çakan, D. Moeller, T. Arts, The effect of periodic ribs on the local aerodynamic and heat transfer performance of a straight cooling channel, ASME J. Turbomachinery 120 (1998) 368–375.

[9] B. Bonhoff, S. Parneix, B.V. Johnson, J. Schabacker, A. Bölcs, Experimental and numerical study of developed flow and heat transfer in coolant channels with 45 degree ribs, Internat. J. Heat Fluid Flow 20 (1999) 311–319.

[10] Y.J. Jang, H.C. Chen, J.C. Han, Flow and heat transfer in a rotating square channel with 45 deg angled ribs by Reynolds stress turbulence model, ASME J. Turbomachinery 123 (2001) 124–131.

[11] S.W. Chang, L.M. Su, T.L. Yang, Heat transfer in a swinging rectangular duct with two opposite walls roughened by 45° staggered ribs, Internat. J. Heat Mass Transfer 47 (2004) 287–305.

[12] Y.J. Jan, S.W. Chang, C.C. Lee, Vortex drafting in narrow channels with two opposite walls roughened by transverse ribs □ FEM approach, Private communication, 2003.

[13] Editorial Board of ASME J. Heat Transfer, ASME J. Heat Transfer 115 (1993) 5–6, Journal of heat transfer policy on reporting uncertainties in experimental measurements and results.

[14] F.W. Dittus, L.M.K. Boelter, Publications in Engineering, vol. 2, University of California, Berkeley, CA, 1930, p. 443.